e-Journal of Nondestructive Testing - ISSN 1435-4934 - www.ndt.net
20th WCNDT 20th World Conference on Non-Destructive Testing
Songdo Convensia, Incheon, Korea, 27~31 May 2024

The Use of Thermal Data for Quality Assurance in the Process of Continuous Ultrasonic Welding of Thermoplastic Composite Materials

D. GÖRICK[1,*], L. LARSEN[1], I. STINGL[2], D. BAUMBACH[2] and A. SCHUSTER[1]

[1] Center for Lightweight Production Technology, German Aerospace Center (DLR), 86159 Augsburg, Germany, Dominik.Goerick@dlr.de, Lars.Larsen@dlr.de, Alfons.Schuster@dlr.de
[2] Institute of Optical Sensor Systems, German Aerospace Center (DLR), 12489 Berlin, Germany, Dirk.Baumbach@dlr.de, Isabelle.Stingl@dlr.de
*Contact: Dominik.Goerick@dlr.de

Abstract
Continuous ultrasonic welding (CUW) is a manufacturing process used to join thermoplastic composite materials using high-frequency ultrasonic vibrations. Under pressure and vibration, the welding material heats up, melts and the welding partners are joined while they are cooling down. The development of CUW is getting raised attention over the last decade since the use of thermoplastic composites (TCs) in the production industry and especially the aerospace sector demands for economic and fast joining techniques. In order to establish this welding technique in the industry it is necessary to develop methods which enable to do quality assurance on the produced welding seams. In the experiments described in this paper the potential of thermal measurements for the quality assurance of the ultrasonic welding of TCs is investigated. Different thermal systems are evaluated and it is described how the data of the most promising technique is further processed and fed to an artificial intelligence (AI) algorithm. The here trained networks are created to predict lab-shear-strength values and reach mean absolute error scores of below 1 MPa. The described investigations hint that thermography seem to be a valuable resource to make more reliable quality assurance in the process of CUW of TCs and therefore might help to establish the use of this welding technology further in the industry.

Keywords: Continuous Ultrasonic Welding, Artificial Intelligence, Deep Learning, Quality Assurance, Infrared Camera, Thermography

1. Introduction

1.1 Technique of Ultrasonic Welding

Ultrasonic welding of TCs stands as a specialized technique applied to join composite materials. The technique is favored in industries where lightweight and robust composite materials, often reinforced with fibers like carbon or glass structures, are in widespread use. Especially in the aerospace and automotive industries it is getting raised attention [1]-[5] due to the fact that many components are supposed to be built out of TCs.
Ultrasonic welding of TCs offers several noteworthy advantages which enhances the already raised attention on this technique. For example, it is known for its speed and efficiency [6] while having minimal energy consumption. In addition, it eliminates the need for adhesives or additional materials, thereby reducing the risk of contamination. The process is highly precise and leads to strong, dependable joints. Moreover, it can be easily automated, making it a suitable choice for various manufacturing processes.
Ultrasonic welding relies on the application of high-frequency ultrasonic vibrations to start the bonding process. At its core, ultrasonic welding operates on the principle of converting electrical energy into mechanical vibrations and applying these vibrations to the welding specimens through a device known as sonotrode. The welding apparatus is composed of a converter, a booster and a sonotrode/ horn. While the converter transforms an electrical signal into mechanical oscillations [6]-[8], the booster provides the opportunity to amplify the created mechanical oscillation. The horn vibrates at the created ultrasonic frequencies, typically ranging from 15 to 50 kHz [8], [9], and transfers the oscillations in the welding parts [6], [7]. In the

 https://doi.org/10.58286/29934

joint area, where the bonding has to occur, these high-frequency mechanical vibrations generate heat through friction [9], [10] which leads to localized softening and melting of the material. As the horn continues to oscillate, the molten material from both components merges, creating a bond between the upper and the lower welding part. Once the ultrasonic energy is cut off, the material cools and solidifies under the application of pressure and is forming a robust welding seam. When the horn is hold steady at one place and is responsible for the heating of the material and for applying the pressure during the cooling, the process is called spot welding. If the horn is moved continuously over the welding specimen and an extra unit, called the heat sink, is lead behind the horn to apply the pressure in the cooling phase, then the process is called continuous ultrasonic welding. Ultrasonic welding of TCs is a sophisticated technique that leverages high-frequency vibrations to bond composite materials effectively and fast. It offers numerous advantages, including speed, efficiency, precision, and the capability to create durable, lightweight joints and therefore making it a valuable asset in industries where composite materials play a significant role in the manufacturing process.

1.2 Artificial Intelligence

AI is a rapidly advancing field within the field of computer science and technology. Its primary focus lies on the development of computer systems with the capacity to perform tasks that usually demand human intelligence. These tasks encompass a wide array of activities, such as problem-solving, learning, reasoning, understanding natural language and even perceiving and interacting with the surrounding environment. The field of AI comprises a multitude of subtopics, including machine learning (ML), natural language processing, computer vision and robotics. [11]

AI systems are engineered to emulate human cognitive functions, and they can be trained to identify patterns in data, make predictions, and adapt to new information by approximating complex systems mathematically [12]. AI technology finds applications across diverse industries and sectors, from healthcare [13] and finance [14] to manufacturing [15] and the development of autonomous vehicles [16]. Its transformative influence is steadily shaping the way humankind engage with technology and holds the potential to address intricate challenges while enriching our daily lives in innumerable ways. These potentials lead to the decision to use AI in the quality assurance process for the welding of TCs.

1.3 Quality Assurance for Ultrasonic Welding

When it comes to influencing the quality of produced welds of ultrasonically welded TCs, there is already done some research about the importance of different welding parameters. Most prominent seem the investigations of Villegas about sonotrode displacement and power data which were measured during the process of spot welding TCs samples [17]. In addition, another research team used a wave transmission model to make statements about achieved welding qualities [9]. As Görick, Schuster, Larsen, et al. already pointed out, the displacement measurement of the horn during a CUW process is not possible since the horn is steadily moving and the conditions below the horn do not change owed to the fact that the material below the horn is always in the status of melting [18]. This leads to the conclusion that the different welding stages, described by Villegas [17] or Li, Liu, Shen, et al. [9] are not stepped through while the horn is over one position of the welding sample and measuring displacement is not possible in case of CUW. Many of the other investigated parameters, which are reported to have an influence on the welding quality, are parameters which are set to induce the welding process and therefore are not able to show influence of defects in the welding zone or similar problems

which might occur during the process of welding [18]. Nevertheless, some investigations were done about welding parameters which could be already recorded during a weld and their potential to be of use for an AI training was evaluated [19]. Since the investigated parameters looked suitable to be used for a bigger AI training experiment, more samples with an extended set of recording parameters were created and used in order to train an algorithm to predict the welding quality [20], [21]. Nevertheless, the trained algorithms reached accuracies in quality classification of slightly above 70 % [20], [21]. This result can be interpreted as a first step in the right direction, but the authors pointed out that further investigations with even bigger data sets have to be proceeded and that it may be possible that the recorded parameters do not carry enough information to give the algorithm the opportunity to approximate a connection of the data and the weld quality [20], [21].
Based on this statement, new input parameters, which correlate with the welding quality, were investigated [18]. In the mentioned study the parameters welding sound (measured sound signals while the welding takes place) and thermography images are described to be of use for the quality prediction of ultrasonically welded TCs. TCs-samples were spot welded together and a thermographic image was acquired a short time after the horn lifted from the welding sample. From each image the mean temperature is calculated and correlation coefficients between the mean temperatures and the lab-shear-strength (LSS) values of all samples were calculated. Medium correlation between mean temperature and LSS value was found for these described investigations [18]. In addition, the authors describe the use of the temperature data (alongside of sound- and welding time data) for the training of different ML algorithms to predict whether a welding is good or bad. Classification rates of over 90 % were archived with the trained networks. The article points out that the investigations were done with spot welded samples only and that there are challenges to overcome in order to apply quality assurance of ultrasonically welded TCs plates when it comes to CUW. Main reason for these challenges is the fact that in spot welding the whole system is static while in CUW the welding head moves over the sample and there are many images of one and the same area of the welding seam. Since thermal data seem to carry the potential to be of great support for the quality assurance in ultrasonic welding [18], the experiments in this paper make a generalized approach at the topic of thermal measurements in the process of CUW by investigating different measuring techniques and evaluating their use for quality prediction with AI. The most promising technique will be used to train an ML-algorithm to predict the LSS value of welded TCs.

2. Principles and Methods

2.*1 Welding Setup*

For ultrasonic welding of TCs two or more welding partners have to be placed on an anvil with at least one area of overlapping structure. The overlapping structure usually builds the area where the connection of the welding specimen will take place and is called welding zone. Between the welding partners an energy director (ED) can be placed in order to provide an interface where the heat is generated [7]. Usually the ED is consisting of the same material as the matrix of the welding plates. Clamps are used to fixate the welding components on an anvil. At the German Aerospace Center (DLR) the welding apparatus is mounted to a *KUKA* robot (KR300 R2500 Ultra Robot) in order to be able to move the horn over a welding seam and apply the necessary welding forces. When the technique of CUW is used, the welding head has a compaction roller mounted in front of the horn and a heatsink mounted behind the horn. The compaction roller pre-compacts the welding samples and the heat sink is used for applying pressure on the welding seam while it is cooling down. The whole welding system and its

sensors are connected to a Beckhoff bus system with communicates with *TwinCat* (Beckhoff, Germany). All parameters for welding are set within this system as well as most of the measurable parameters are recorded by the TwinCat system. The welding head originates in the work of Engelschall at DLR in 2018 [22], [23].
For the proceeded trials in this paper TCs plates made of carbon fibres (T700G) which are embedded in low-melt polyaryletherketone (LM-PAEK). The original plates had dimensions of 1200 mm x 1800 mm x 1.96 mm and a fibre layup of $[45/90/135/0/45/135/0]_s$. The plates are water jet cut in welding plates with dimensions of 104.6 mm x 378.2 mm. Water jet cutting is the preferred cutting method for this processing step in order to keep the load on the plates as small as possible and to avoid fraying of the fibres. The welding plates are cut in a way that the fibres building the second layer (90°) are oriented in parallel to the welding direction. The dimensions of the welding zone are similar to the ASTM-D1002 norm which is why the welding zone width is 12.7 mm for all experiments. This dimension defines the overlapping zone of two welding plates. Two stripes of ED are placed in this overlapping area. The ED is fixated with small spot welds which were created manually with an ultrasonic welding head. Special attention is payed to the position of the fixation with the result that each sample, which is later cut from the welded plates, has one fixation spot in its centre. The ED has a width of 11.7 mm and is 0.1 mm thick. For the welding process a horn with a rectangle shape and dimensions of 25 mm × 13 mm is used (horn has round edges with 1 mm radius to each side) and positioned with its longer side orthogonal to the welding direction in the middle of the welding zone. In order to create different welding qualities, the welding parameters are setup in different ranges. For more detailed information see table 1. For each welding trial the plates are placed on the anvil randomly to cover different fibre orientations of the 45° layer. Thermal measurements, which are described in the upcoming section more in detail, are performed during every weld (thermocouples and external thermography was not used in every welding process). Each welding experiment results in one welded plate which can be cut in 13 samples which results in 585 samples (45 welds). With orientation on the ASTM-D1002 norm the plates are water jet cut into 25.4 mm wide samples with a length of 190.5 mm. In the cutting process the first and the last 10 mm of the welded plate are cut off. LSS tests are performed with a *Zwick/Roell* (Retroline 1475, ZwickRoell GmbH & Co. KG, Germany, Ulm) testing machine with 20 kN clamps (ZwickRoell GmbH & Co. KG, Germany, Ulm) and a cross head speed of 1.3 mm min^{-1}.

Table 1. Different welding parameters and their ranges or fixed values for all proceeded experiments.

Parameter	Range	Unit
Amplitude	74-100	%
Welding Horn	600	N
Heatsink	5	bar
Compaction Roll	300	N
Welding Velocity	17 or 20	mm s^{-1}

2.2 Temperature Measurements

2.2.1 Setup of Thermocouples

With the use of thermocouples, it is investigated whether the temperature distribution and development during the welding process can be measured. A thermocouple is a sensor that consists of two wires of different materials connected at one end. This connection point is then mounted on a measuring point while the free ends are connected to a multimeter (for the here described trials two *HIOKI LR 8400-20* are used). For different temperatures at the measuring point, differences in voltage will occur on the multimeter due to the thermoelectricity. This phenomenon is also known as the Seebeck effect [24], [25]. By specifying the thermocouple type in the multimeter, the temperature at the measuring point is calculated directly by the system. The thermocouples used were type K, with double insulated wires and assembled to one wire, coated with glass silk. In order to be able to measure temperatures in the interface between TCs plate and anvil (areas on which no infrared camera has direct view) a shim plate was manufactured and placed between anvil and TCs plate. This shim plate has cut-outs for the thicker glass silk insulated cables of the thermocouples to introduce as little geometry as possible into the interface (see figure 1 plate C and D). However, the wires of the thermocouple with the measuring point had to be placed directly in the interface between plate and anvil in order to be able to measure the temperatures at this point. Temperatures are measured at 60 measuring points, 27 of which were on the shim plate in the interface, 28 on the surfaces of the TCs plates, 2 for ambient temperature measurement and one measuring point each on roller, sonotrode and heat sink. The measuring points on the TCs surfaces are directly above the measuring points on the shim plate. The positions of the measuring points on the TCs plates are shown in figure 1 (plates A and B) and in the interfaces on the shim plate in figure 1 (plates C and D). The distances between the measuring points in welding direction are approx. 39 mm. The distance to the joining zone centerline varies between approx. 0 mm (on the shim plate, directly under the joining zone), 10 mm (directly besides the welding zone on top of TCs), 30 mm (a), 45 mm (b) and 95 mm (c). All thermocouples are fixed with Kapton tape in position. The temperatures are measured with a frequency of 10 Hz at every thermocouple. For more detailed description of the thermocouple measurement please read [26].

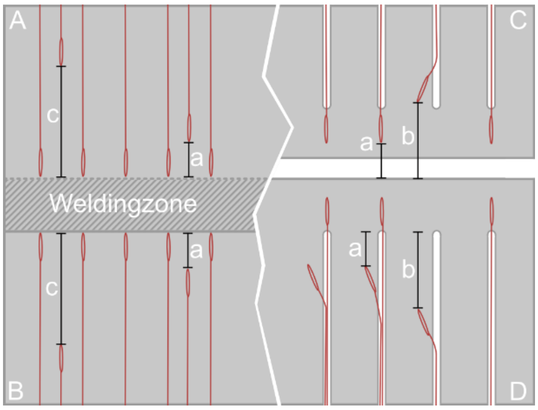

Fig. 1 Schematics of thermocouple measuring points on TCs plates. In red: Thermocouples. Left side shows the welding plates while right side shows the plate below the welding samples.

2.2.2 Setup External Infrared Camera

To investigate the whole welding seam, a multi-camera setup consisting of a panchromatic stereo camera system and an *Optris PI 640* long-wave infrared camera including an additional near infrared lighting is mounted at a distance of approx. 81 cm from the weld seam. When the camera is focused at 100 cm, a ground-resolved distance of approx. 2.1 mm can be expected at a working distance of 81 cm, as the study of Wischow, Dahlke, Meißner, et al. [27] shows. Depending on the application, the camera can operate in different temperature ranges. For the experiments a temperature range of 0-250 °C is chosen. The infrared camera works in the spectral range of 8-14 µm, has a horizontal field of view (FOV) of 90° and is aligned to the scene at an angle of approx. 30°. The raw data is read out as 640 times 480 pixel video stream at a frequency of 32 Hz using the manufacturer's *PIX Connect* software [28] (Optris, Germany).
2.2.3 Setup FLIR

For a close investigation of the welding seam after the melting of the material took place, a *FLIR A35* (Teledyne *FLIR*) thermography camera is mounted to the welding unit. The thermography camera has an approximate viewing angle of 45° and records the welding horn, the area behind the horn and the first section of the heatsink. Image acquisition is realized with *TwinCat Vision* (Beckhoff, Germany) which can be implemented in the controlling software of *TwinCat* which manages the general welding process. Every 500 µm change in x-position of the tool center point (TCP) the camera acquires a 16-bit monochrome tiff-image and stores it to the system. The TCP is located in the middle of the welding horn. Position coordinates of the TCP are also used to name the recorded image so a x-position can be connected to each image. Since it is expected that the melting temperatures do not completely reach the surface, *HighGainMode* is selected in the camera registry. This means that the camera has a finer temperature resolution but measures smaller temperature space for measurement [29].

2.3 AI Methods

Processing of the data for AI training is done with Python 3. For different processing steps some of the most common data processing libraries are used. Namely these libraries are Matplotlib [30], NumPy [31], Pandas [32] and OpenCV [33] for Python. For creating artificial networks, the library Keras [34] with TensorFlow [35] is used while some of the statistic calculations are done by SciPy [36]. The documentation of different training approaches is recorded with MLflow [37] and hyperparameterization is done by Optuna [38].

2.4 Data Processing and Evaluation

2.4.1 Thermocouples

For the processing of the thermocouple data there is no specific image but in recordings of the *FLIR* camera some of the thermocouples can be seen (see figure 2, white circles). Welding direction in the image is from right to left. Some of the thermocouples are visible as bright specs when compared to their surrounding environment and it seems that the wires of the thermocouples are moving caused by the welding process and thereby generate heat. If this hypothesis is true it would mean that the thermal measurement is not reliable because heat is generated at the measuring system itself. During the experiments, it was observed that some of the thermocouple wires became detached from the TCs surface or that the connected wires became loose or even broke, so that they no longer formed a measuring structure and could not measure temperatures. The thermocouples which are used for measuring temperature under the welding zone were melted in the plate with which they had contact. A temperature recording by the thermocouples is shown in figure 3 where the welding took place at > 85 s and < 110 s. In these measurements some of the signals seem to be unrealistic high or low (> |1000| °C, see figure 3 graph on top). Some of the thermocouples had detached wires which leads to an infinite resistance which is why these sensors are supposed to be responsible for these extreme measurements. When excluding all measurements which had temperatures over 500 or below -10 °C as seen in figure 3 (graph in the middle), there are some high and edgy temperature signals which reach over 200 °C, visible. These signals might come from internal friction at the thermocouple. Some of the lower temperature measurements get visible, if these values are also excluded from the plotting (see figure 3 graph at the bottom).

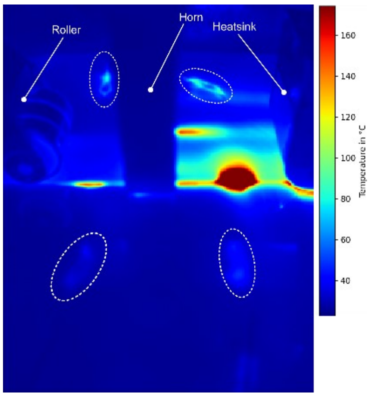

Fig. 2 **Heating of thermocouples during the welding process. Thermocouples are circled with white-dashed lines. The temperature scale should only be considered relatively, not absolutely. (Figure inspired by [26]).**

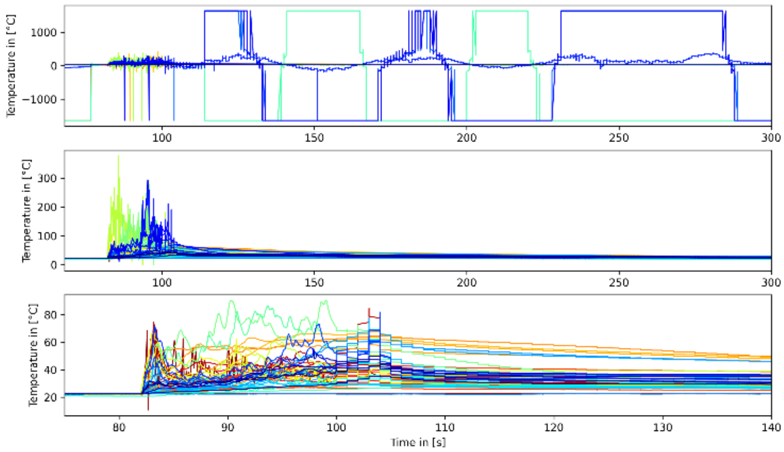

Fig. 3 **Thermocouple measurement of welding No. 9. First plot shows the temperature measurement of all thermocouples. Second plot shows all measurements which had maximal temperatures below 500 °C and minimal temperatures of above -10 °C. Plot three shows all measurements which had maximal temperatures below 100 °C and minimal temperatures of above -10 °C. Notice that the time scale in the last plot is different to the other plots.**

2.4.2 External Infrared Camera

The raw data output from the external infrared (IR)-camera is a video sequence of about 20 seconds, recorded from the static IR-camera placed next to the robot and welding table. The video stream is converted into individual images and time periods of interest are extracted. Figure 4 shows an example of two images of welding attempt No. 9 at different time steps, where the welding direction runs from right to left. In figure 4a the welding process is active, which means that roller, welding horn and heatsink have contact to the surface of the welding material. In addition to the temperature progression on the weld seam, thermal reflections on the material surface next to the actual weld can be seen, for example the reflection of the roller in the middle on the left side of figure 4a (white circle). In figure 4b the welding is already completed. The horn is retracted, roller and horn are no longer visible in the thermal image. Only the heat sink is still in contact with the material surface. Comparing the measured temperatures in both images, the rapid drop in maximum temperatures after the end of welding can be seen (max. temp.: > 200 °C in figure 4a, > 100 °C in figure 4b). Both images show that the acquired data provide a good overview of the welding seam and therefore make it possible to investigate the general warming and cooling behavior of the seam.

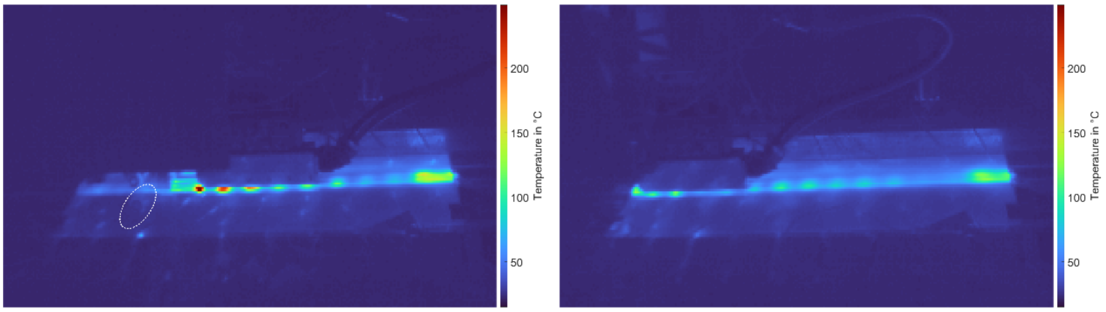

(a) (b)

Fig. 4 Thermal camera image of entire welding attempt No. 9: (a) Active welding where roller, horn and heat sink are in contact with the surface with measured temperatures above 200 °C. White dashed ellipse marks a weak reflection of the compaction roll in front of the sonotrode. (b) Finished welding where roller and horn have no contact with the weld seam while heat sink is still in contact to the surface. From (a) to (b) the maximum temperature dropped quickly.

2.4.3 FLIR Data

During the experiments the *FLIR* camera showed itself to deliver the most detailed data which also were good to match to an x-position on the welding plate due to the fact that the TCP is saved in each image name. This is why it was decided to develop a preprocessing code in order to transform the data to be able to make exploratory data analysis (eda) and AI-training.
Images are recorded in a format of 320 times 256 pixels with the robot-TCP position stored in the name of each image. Each image is a 16-bit deep gray-scale image. In order to get the temperature values the first two bits have to be bit-masked off before equation 1 [39] is applied to each pixel value (see figure 5). Since the surface of the samples is observed, lower temperatures are expected and the camera is set to *HighGainMode* [29] which has a temperature range of -25 up to 135 °C. As displayed in figure 5 the calculated temperatures seem to exceed 135 °C and the upper cutoff seem to be around 170 °C. This extended range may be possible since the camera sensor data are recorded not by the camera software provided by the manufacturer but with a custom program executed in *TwinCat Vision*.

$$T_{[k]} = \frac{B}{ln\left(\frac{R}{S-O}+F\right)} \qquad (1)$$

In equation 1 S represents a pixel value while the other letters are camera intern registry parameters. After the use of equation 1 the temperature values are in Kelvin so an additional shift is done to have the temperature values in °C. When these steps are done each image stores information about the measured temperature in °C. Notice that in the following paragraphs the term “image” is used to explain the preprocessing steps further. The images are only shown for explanatory purposes, the real data is stored in two dimensional tensors. Since the camera recordings show not only the welding zone but also the surrounding area, the region of interest (ROI) has to be cut from the original sized images. During this cutting process the distortion of the images is also eliminated by applying a transformation matrix (equation 2) which was calculated by OpenCV [33]:

$$trans_{mat} = \begin{bmatrix} 4.16603031 \times 10^{-2} & 1.99969455 & -3.17034906 \times 10^{2} \\ -1.61185986 & -2.64239321 \times 10^{-2} & 3.55454735 \times 10^{2} \\ -2.23909242 \times 10^{-3} & -6.68095185 \times 10^{-5} & 1.00000000 \end{bmatrix} \quad (2)$$

The whole process of how the ROI with the corresponding temperature data is extracted from the raw data is schematically shown in figure 5. After the thermal information are transformed,

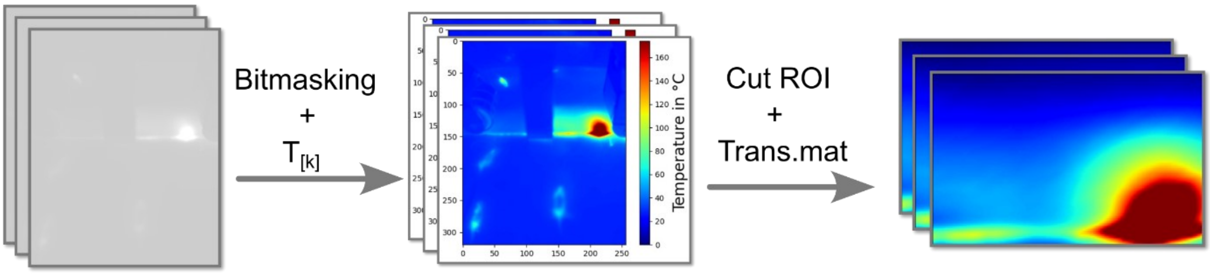

Fig. 5 Step 1 of data processing. Data of the raw thermographic images are bitmasked and the resulting values are transformed with an equation to get temperature values. The ROI is then cut from the thermographic images and are transformed in order to eliminate perspective distortion.

the question arises how the data have to be processed further in order to retrieve condensed information for eda or AI training. At the moment the data for each welding seam is three dimensional. Two dimensions are defined by the pixel height and width and the third dimension is the temperature information dependency of the TCP position which itself has similarities with time. The goal of the next processing step is to reduce the dimensionality, to get one image of the welding zone which is representative for a temperature measurement at one point of time after the welding took place. This reduction can be done by extracting from each image the same column of pixels and then connect the extracted columns with their real position on the welding plate (see figure 6).

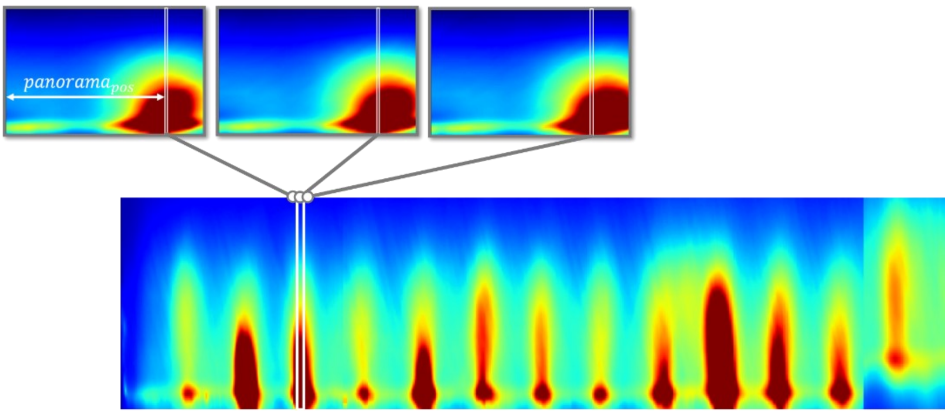

Fig. 6 Step 2 of data processing. From each ROI image a pixel column is extracted and concatenated to one thermographic panorama. $panorama_{pos}$ defines the extraction position in each image.

In order to create the panorama image, the real position of an extracted column has to be calculated with the help of the TCP. Since the distance of the ROI to the horn can be measured in an image and the distance of the extraction column from the left edge of an image ($panorama_{pos}$) is defined manually, x-position data of each column can be calculated and saved with the thermographic data. The scale for all calculations (used to calculate from pixels to mm

to get the distance from horn to ROI in mm and to get panorama$_{pos}$ in pixels) is created on basis of one of the thermal images and the knowledge about the width of the horn. This method bares the danger of inaccuracy due to resolution and a small error calculation is proceeded:
The TCP position of the starting point is saved by the system. Since the horn is placed on the welding plates in a way that its edge is congruent with the welding plate the real position of the beginning of the welding plate can be calculated by equation 3:

$$x_{startReal} = TCP_{start} - \frac{HornWidth}{2} \, [mm] \tag{3}$$

To calculate now the error of the scale, a thermal image is taken where the edge of the plate is visible and a scale is created with the help of the horn width since that dimension is known. The scale can then be used to measure the distance from the right horn edge to the edge of the welding plate ($\Delta X_{HornToEdge}$). With this value and the knowledge of the width of the horn the theoretical starting position ($x_{startThermo}$) can be calculated with equation 4:

$$x_{startThermo} = TCP - \frac{HornWidth}{2} - \Delta X_{HornToEdge} \, [mm] \tag{4}$$

By subtracting the starting position calculated with the thermal image from the real starting position an error of this method can be defined. For the measured data, the error is approximately 1.571 mm.
The welded plates are water jet cut into LSS-samples with a width of 25.4 mm. According to the real cuts of a welding plate, the created thermographic panoramas have to be cut the same way. With respect to the cut off zone at the beginning and the end of a welded plate, the panorama image is cut in 13 smaller images which are each connected to a real LSS sample and therefore can be labeled with an LSS value (see figure 7).

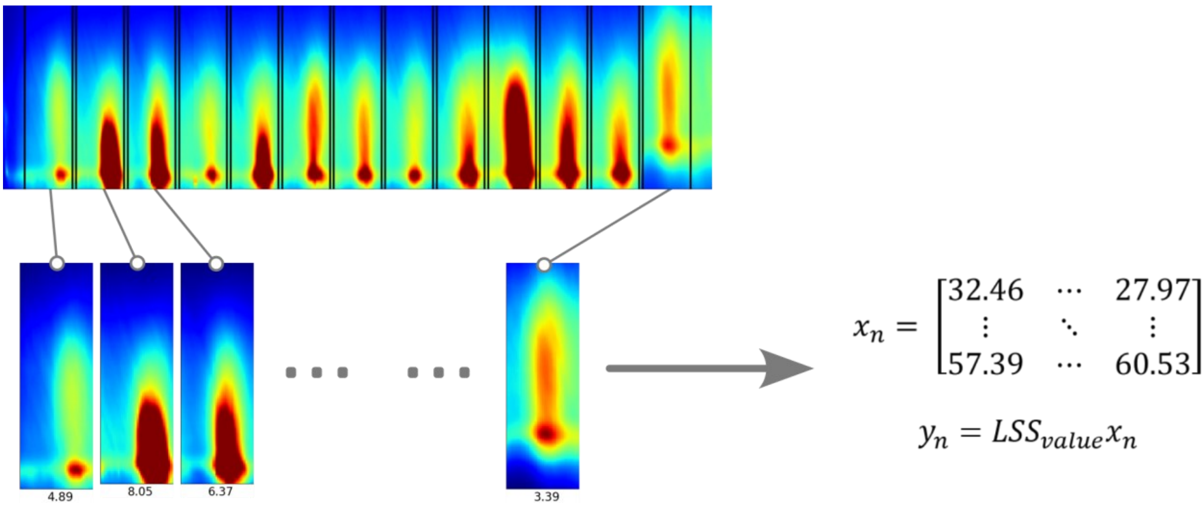

Fig. 7 Step 3 of data processing. The thermographic panorama is cut accordingly to the samples which are cut from the welded plate. After cutting, each sample has a thermography image and a label which can be stored in a matrix x and a value y.

Every image is stored as a two-dimensional tensor in the system as a NumPy data tensor while its label is used to name the stored file. In a first step eda is performed with the created data. Weld experiments with No. 0, 5 and 20 are excluded from these investigations due to the fact that the recordings were faulty. In addition, some samples are excluded if the algorithm used for labeling the samples, did not find a stored LSS value for a sample. This leads to a total of 543 samples for investigation. Goal of the eda is to investigate if there is a correlation between the measured temperature and the achieved welding quality/ LSS value. To simplify this investigation the image data is further reduced as described by Görick, Schuster, Larsen, et al. [18] by calculating the mean temperature of each image. Spearman- and Pearson correlation coefficients are then calculated for the whole set of data. In addition, the correlation coefficients are also calculated for a data set where the first and the last sample are eliminated from the set which lead to a set size of 460. In a final step all image data are stored randomly in a three-dimensional tensor which then is used to train and test ML algorithms. Similarly, the labels are stored in a one-dimensional tensor at equivalent indexes. For the storing of image data, it has to be mentioned that not all images have the same size and are therefore augmented with zeros to their right side in order to have the same size as the largest image in the data set. The variation in size originates from the trigger mechanism in a way that not for each LSS sample the same number of images is recorded (discretization leads to non-equidistant camera triggering).

2.4.4 AI Training with FLIR Data

The correlation analyses for the data set without the data of the first and last LSS sample of each weld show larger correlation (see table 3) which is why this data set is used for the AI algorithm development. Before the generated data can be used for AI training, all values are normalized. Training is done with 300 samples while 100 samples are used for the validation process and 60 samples for final testing. The final input image size was 127 times 44 pixels, with zero values on the right side if the original image had less pixel columns. For the processing of data, a two-dimensional neural network (2D CNN) is used. The network is composed of three convolution layers with a max pooling layer between each convolution. Connected to the last convolution layer is a flatten layer to transform the data in an input shape which can be fed in a dense layer. Since a regression network is trained, the last layer is a dense layer with one neuron. Training was proceeded with the rmsprop optimizer and for optimization the mean square error (mse, see equation 5) is observed and minimized.

$$mse = \frac{1}{n}\sum_{i=1}^{n}(y_i - \hat{y}_i)^2 \quad (5)$$

For testing and as an optimization return value for the hyperparameterization with Optuna, the mean absolute error (mae, see equation 6) is used.

$$mae = \frac{\sum_{i=1}^{n}(y_i - \hat{y}_i)}{n} \quad (6)$$

Here n represents the number of sample while y_i is the label of each sample and $\hat{y}_i$ stands for the value predicted by the network. To reduce the computational cost not all hyperparameters are fully optimized with Optuna. Before the full hyperparameterization took place the general importance of all hyperparameters is evaluated with the help of Optuna and only the parameters with an importance of equal or greater 3 % are set for optimization in the final training approach. All other parameters are set to the value which is supposed to be the best value during the importance study. Parameters for importance evaluation for a convolution layer are *number of filters*, *filter size* and *activation function* and for a dense layer *number of neurons* and *activation function*. The max pooling layers are excluded from this investigation but *epoch number* and *batch size* are also evaluated. For the evaluation of importance 100 trials are performed. The importance evaluation of the different parameters is listed in table 2. After the important hyperparameters are defined in the system, final training with hyperparameterization is performed in 500 training attempts. For this training an early stopping callback function is implemented to monitor the loss function. If the function value does not reduce by at least 0.001 for 10 epochs in a row, the training is stopped and the weights of the best training epoch (in this case 10 epoch in the past) are recovered and saved. This functionality starts observing the loss function at epoch No. 15. The best training result is found by looking for the smallest mae value of all 500 trained networks.

Table 2. Importance of different hyperparameters of the trained neural network. Importance is rounded with decimal precision of 10^{-4}. If no value is defined the parameter is set to be dynamic for the hyperparameterization in the final training attempts.

Parameter	Set Vale	Rel. Importance
filter_size_3	-	0.5986
filter_size_2	-	0.1558
activation_2	-	0.0578
filter_size_1	-	0.0472
activation_4	-	0.0386
batch size	-	0.0305
activation_3	softmax	0.0147
activation_1	softmax	0.0143
number_filters_3	32	0.0122
number_filters_2	30	0.0111
epochs	95	0.001
number_filters_1	59	0.0075
neurons_dense_1	4	0.0026

3. Results

3.1 Thermocouples

Some of the measured temperatures extend beyond temperatures of the welding process and indicate that the vibrations can permanently destroy the thermocouples. In addition, most of the thermal measurements seem to measure the friction of the thermocouples on the surface rather than measuring the temperatures which result from the actual welding process. Due to that, the method of temperature measurement with these thermocouples appears to be unsuitable for the ultrasonic welding processes.

3.2 External Infrared Camera

Thermal images are taken with a static IR-camera system at a greater distance from the weld seam and with a larger FOV compared to the *FLIR* camera, making it possible to monitor the entire welding seam. In this way, heating- and cooling processes in the material can be observed before and after the actual welding. This data can be helpful for evaluating the welding quality. However, a larger FOV also means an increased susceptibility to thermal reflections from different materials or other temporary heat sources. In order to obtain more plausible temperature information, the emissivity of the material in the scene to be observed has to be set in the software beforehand. This can be challenging due to different materials within the scene. Due to the limited resolution of the IR-camera and the associated ground-resolved distance, fine details in the temperature progression of the welding process are difficult to detect. The use of optics with a narrower FOV (e.g. 30°) at a closer distance to the weld seam could be investigated in order to reduce possible reflections and get a higher resolution thermal measurement. In addition, the data shape may have the potential to be reshaped in a way that the data can be fed into an AI algorithm and provide the algorithm described above with additional information about the cooling process.

3.3 FLIR Data

The in this paper introduced method for prepossessing the recorded thermal data of a continuous ultrasonic welding process seem to be accurate enough to be used for data analyses. Mean temperature values of each image plotted against the LSS value are shown in figure 8. For all visualized values there seem to be a trend that with a higher mean temperature the welded connection gets stronger. Nevertheless, the LSS value distribution of the points at higher temperatures gets larger (see figure 8a)). If the first and last welding sample of each weld experiment are eliminated (this data set is called *reduced data set* from here on) from the visualization, the LSS value distribution towards higher temperatures gets smaller and the trend that higher temperatures are connected to higher LSS values gets more prominent (see figure 8b)).

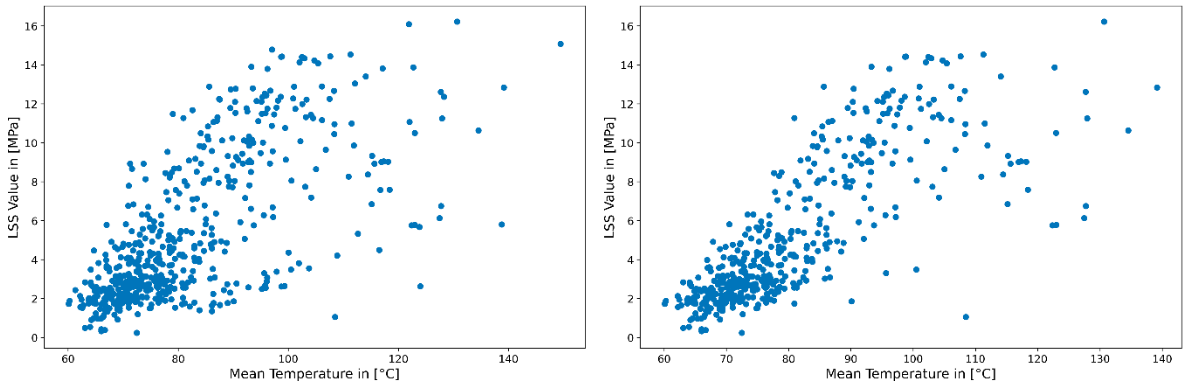

(a) (b)

Fig. 8 Mean temperature of each thermal image plotted against the LSS value. (a): All samples. (b): Samples plotted without the first and the last sample of the welding plate (start and ending of the welding process).

These observed trends are also supported by the calculation of the Spearman- and the Pearson correlation coefficient (see table 3). In all tests medium correlations are calculated with p-values lower $\alpha = 0.05$ which leads to rejection of H_0 and real correlation can be assumed. Since the correlation value of the Spearman correlation for the reduced data set is larger than 0.8, the correlation is supposed to be large [40].

Table 3. Correlation coefficients of the mean temperature against the LSS values with (All Samples True) and without (All Samples False) the first and last sample of each plate. Values rounded to 10^{-4} precision.

Correlation	Corr. Coefficient	p-value	All Samples
Pearson	0.6879	2.5405×10^{-77}	True
Pearson	0.7879	1.6961×10^{-98}	False
Spearman	0.6988	9.3344×10^{-81}	True
Spearman	0.8186	2.1934×10^{-112}	False

In case of AI training the best trained network achieved a mae score of 0.06 which is equivalent to 0.979 MPa if the value is transformed back to the LSS value. A visualization of the networks prediction against the ground truth is shown in figure 9. The trained network seems to learn from the given data and the predictions and the ground truth lay in most cases relatively close together.

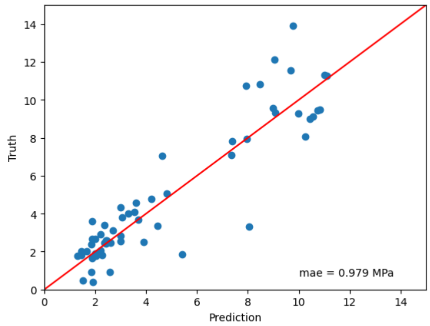

Fig. 9 Predicted LSS values plotted against the ground truth. Red line indicates the optimal location of each point where prediction and label are the same.

4. Discussion

It seems that thermography offers good opportunities to be used for the quality assessment of ultrasonic welded TCs. Nevertheless, there are a few thoughts to keep in mind. The here described use of thermocouples seem to be the only investigated technique which leads to non-reliable data based on the fact that the thermocouples generate friction themselves and therefore do not measure the heat which is resulting from the welding process. It may still be possible to connect the thermocouples in another way to enable reliable measurement of the welding temperatures.
The external IR-camera provides good overview of the whole welding sample but the data could not be used for AI training due to the fact that the x-position of camera and welding sample could not be matched in a detailed enough scale. If the matching can be done in a more detailed manner and a process for transforming the more complex data of the external IR-camera into an appropriate shape for an AI-algorithm is designed, the global cooling process of the welding samples might be of use for the generation of additional AI training data.
The *FLIR* data is used for detailed quality assessment of the welding process. The camera is set up to a smaller measurable temperature range with a higher resolution since it was expected that the welding specimens surface reaches smaller temperatures. This leads to a temperature cut off and some of the thermal information could have gone lost or are measured inaccurately since the calibrated temperature range is exceeded during the experiments. For future measurements it might be advisable to use a different setup of the camera in order to measure temperature more accurately. Nevertheless, this point seems to be not of most importance since the algorithms learn from the data even if they have a cut off in temperature range and temperatures over 135 °C are measured less accurately. A more detailed temperature resolution could lead to an even better network. In addition, the processing of the thermal images is done to generate more understanding of causality but might not be necessary for the training of an AI algorithm. With larger sets of data, it may be possible to give the algorithm stacks of thermal images where the according welding sample is shown and let the algorithm learn which areas of the stacked images are of importance. To investigate this statement a much larger data set is necessary.
The welding process itself was done with samples which had many hand-fixations of the ED. In the thermal data it is seen that these fixations cause heating areas while the areas next to these heating areas remain significant colder. Further investigations should be done without these fixations since they seem to influence the welding. Another point worth mentioning is

that the archived LSS results are relatively low compared to the spot welds described by Görick, Schuster, Larsen, et al. in [18]. This limits the networks ability to recognize stronger welding connections. Since the algorithm in [18] is able to see differences between good and bad welds, where good welds are supposed to have an LSS value of equal to or over 37 MPa, it may also be possible to train an algorithm with the here proposed methods to differentiate in a larger range of qualities. The LSS values in general are relatively low which might be a result of the hand fixations in the welding zone and a weak generator but the here presented results strengthen the statement that quality assurance of CUW of TCs is possible. Further investigations with a larger data set and a larger difference in welding quality should be created in order to be able to make a more generalized statement but it seems that IR-camera images of the welding process help with the quality assurance of the CUW process.

5. Conclusions

In the here presented research different thermographic measurement methods are introduced to the process of CUW of TCs. The measurement of thermographic data with IR-cameras seem to have high potential to the quality assessment of produced welds. Most promising is the data recorded close to the welding zone which leads to the conclusion that this system will be further used to record data during the welding process. Some of the described processing steps generate good understanding of the recorded data set in general but might be reduced in complexity in further trials. In order to get a more reliable and safe AI algorithm, a larger data set with more diverse data should be created but the presented results already help to even the way for the establishment of the CUW of TCs in manufacturing.

Author Contributions: Conceptualization, D.G.; data curation, D.G. and I.S.; formal analysis, D.G.; investigation, D.G.; methodology, D.G.; resources, L.L. and D.B.; software, D.G.; visualization, D.G.; supervision, A.S. and L.L.; funding acquisition, L.L.; writing—original draft, D.G.; writing—review and editing, A.S., L.L., D.B. I.S.; All authors have read and agreed to the published version of the manuscript.

Funding

This research was funded by Bundesministerium für Bildung und Forschung grant number 01IS22018B.

Bundesministerium
für Bildung
und Forschung

References

[1] S. Arul, L. Vijayaraghavan, and S. K. Malhotra, "Online monitoring of acoustic emission for quality control in drilling of polymeric composites," Journal of Materials Processing Technology, Vol. 185, pp. 184–190 (2007), DOI: 10.1016/j.jmatprotec.2006.03.114

[2] R. Slayton and G. Spinardi, "Radical innovation in scaling up: Boeing's dreamliner and the challenge of socio-technical transitions," Technovation, Vol. 47, pp. 47–58 (2016)

[3] K. K. Chawla, "Carbon fiber composites,". New York, NY: Composite Materials: Science and Engineering (2nd ed.), Springer, pp. 252–277 (1998), ISBN: 978-1-

4757-2966-5, DOI: https://doi.org/10.1007/978-1-4757-2966-5_8

[4] R. Marani, D. Palumbo, U. Galietti, E. Stella, and T. D'Orazio, "Automatic detection of subsurface defects in composite materials using thermography and unsupervised machine learning," in 2016 IEEE 8th International Conference on Intelligent Systems (IS), Sofia, Bulgaria: IEEE, pp. 516–521, DOI: 10.1109/IS.2016.7737471

[5] B. Yang and C. Wang, "Thermal nondestructive testing technology of aircraft composite material," in 2009 9th International Conference on Electronic Measurement & Instruments, Beijing, China: IEEE, pp. 2-557-2–562, DOI: 10.1109/ICEMI.2009.5274495

[6] S. K. Bhudolia, G. Gohel, K. F. Leong, and A. Islam, "Advances in ultrasonic welding of thermoplastic composites: A review," Materials, Vol. 13, No. 6: 1284, 2020, DOI: 10.3390/ma13061284

[7] I. F. Villegas and H. E. N. Bersee, "Ultrasonic welding of advanced thermoplastic composites: An investigation on energy-directing surfaces," Advances in Polymer Technology, Vol. 29, No. 2, pp. 112–121 (2010), DOI: 10.1002/adv.20178

[8] I. F. Villegas, "Ultrasonic welding of thermoplastic composites," Frontiers in Materials, Vol. 6, No. 291 (2019), DOI: 10.3389/fmats.2019.00291

[9] Y. Li, Z. Liu, J. Shen, T. H. Lee, M. Banu, and S. J. Hu, "Weld quality prediction in ultrasonic welding of carbon fiber composite based on an ultrasonic wave transmission model," Journal of Manufacturing Science and Engineering, Vol. 141, No. 8: 081010 (2019), DOI: 10.1115/1.4043900

[10] C. J. Nonhof and G. A. Luiten, "Estimates for process conditions during the ultrasonic welding of thermoplastics," Polymer Engineering and Science, Vol. 36, No. 9, pp. 1177–1183 (1996), DOI: 10.1002/pen.10511

[11] F. Chollet, Deep Learning mit Python und Keras: Das Praxis Handbuch vom Entwickler der Keras-Bibliothek. Frechen: mitp Verlags GmbH & Co. KG, (2018)

[12] V. Lakshmanan, S. Robinson, and M. Munn, Machine Learning Design Patterns: Solutions to Common Challenges in Data Preparation, Model Building, and MLOps. Canada: O´Reilly Media Inc., p. 391 (2020), ISBN: 978-1-098-11578-4

[13] J. Bauer, M. N. Hoq, J. Mulcahy, *et al.*, "Implementation of artificial intelligence and non-contact infrared thermography for prediction and personalized automatic identification of different stages of cellulite," EPMA Journal, vol. 11, pp. 17–29 (2020), DOI: 10.1007/s13167-020-00199-x

[14] L. Cao, "AI in finance: Challenges, techniques, and opportunities," ACM Computing Surveys, Vol. 55, No. 3: 64 (2022), DOI: https://doi.org/10.1145/3502289

[15] S. Fahle, C. Prinz, and B. Kuhlenkötter, "Systematic review on machine learning (ML) methods for manufacturing processes - Identifying artificial intelligence (AI) methods for field applications," in 2020 53rd CIRP Conference on Manufacturing Systems, Elsevier B.V., DOI: 10.1016/j.procir.2020.04.109

[16] S. Grigorescu, B. Trasnea, T. Cocias, and G. Macesanu, "A survey of deep learning techniques for autonomous driving," Journal of Field Robotics, Vol. 37, No. 3, pp. 362–386 (2019), DOI: https://doi.org/10.1002/rob.21918

[17] I. F. Villegas, "In situ monitoring of ultrasonic welding of thermoplastic composites through power and displacement data," Journal of Thermoplastic Composite Materials, Vol. 28, No. 1, pp. 66–85 (2015), DOI: 10.1177/0892705712475015

[18] D. Görick, A. Schuster, L. Larsen, J. Welsch, T. Karrasch, and M. Kupke, "New input factors for machine learning approaches to predict the weld quality of ultrasonically welded thermoplastic composite materials," Journal of Manufacturing and Materials Processing, Vol. 7(5), No. 154 (2023), DOI:

https://doi.org/10.3390/jmmp7050154

[19]L. Larsen, D. Görick, M. Engelschall, F. Fischer, and M. Kupke, "Process data driven advancement of robot-based continuous ultrasonic welding for the dust-free assembly of future fuselage structures," in ITHEC 2020, Messe Bremen, Bremen, Germany: German Aerospace Center (DLR), Center of Lightweight Production Technology (ZLP) (2020)

[20]D. Görick, "An artificial intelligence approach for the joint strength prediction of continuous ultrasonic welds of high-performance thermoplastic composites," Masterthesis, Westfälische Hochschule, German Aerospace Center (DLR), Center of Lightweight Production Technology (ZLP) (2020)

[21]D. Görick, L. Larsen, M. Engelschall, and A. Schuster, "Quality prediction of continuous ultrasonic welded seams of high-performance thermoplastic composites by means of artificial intelligence," in 30th International Conference on Flexible Automation and Intelligent Manufacturing (FAIM2021), Athens, Greece, Vol. 55, pp. 116–123 (2021), DOI: https://doi.org/10.1016/j.promfg.2021.10.017

[22]M. Engelschall, "Industrialization concept and process evaluation of continuous ultrasonic welding in advanced thermoplastic composite production," Masterthesis, Hochschule Augsburg, German Aerospace Center (DLR), Center of Lightweight Production Technology (ZLP) (2018)

[23]M. Engelschall, L. Larsen, F. J. C. Fischer, and M. Kupke, "Robot-based continuous ultrasonic welding for automated production of aerospace structures," in SAMPE Europe Conference 2019 Nantes, France

[24]D. D. Pollock, The Theory and Properties of Thermocouple Elements. Philadelphia: American Society for Testing and Materials, p. 1 (1971), ISBN: 0-8031-0074-4

[25]K. Irrgang and L. Michalowsky (Hrsg.), Temperaturmesspraxis mit Widerstandsthermometern und Thermoelementen. Germany: Vulkan-Verlag GmbH, pp. 23–26 (2004), ISBN: 3-8027-2200-0

[26]I. Stingl, "Thermal modeling, analysis and correlation with testing of continuous ultrasonic welding processes," Masterthesis, FH Aachen - University of applied sciences, German Aerospace Center (DLR), Institute of Optical Sensor Systems (2023)

[27]M. Wischow, D. Dahlke, H. Meißner, I. Ernst, S. Jarka, and R. Glück, "Calibration and validation of a stereo camera system augmented with a long-wave infrared module to monitor ultrasonic welding of thermoplastics," in ISPRS Annals of the Photogrammetry, Remote Sensing and Spatial Information Sciences, XXIV ISPRS Congress (2022 edition), Nice, France, Vol. V-1-2022, pp. 179–186 (2022), DOI: 10.5194/isprs-annals-V-1-2022-179-2022

[28]Optris, optris PIX Connect, <https://www.optris.com/de/produkte/infrarot-kameras/software-pix-connect/>, (9 Nov. 2023)

[29]Teledyne Flir, What Is the Relation between TemperatureLinearResolution and SensorGainMode (Temperature Range) for the FLIR Ax5 Series? <https://www.flir.eu/support-center/instruments2/what-is-the-relation-between-temperaturelinearresolution-and-sensorgainmode-temperature-range-for-the-flir-ax5-series/> (28 July 2023)

[30]J. D. Hunter, "Matplotlib: A 2d graphics environment," Computing in Science & Engineering, Vol. 9, No. 3, pp. 90–95 (2007), DOI: 10.1109/MCSE.2007.55

[31]C. R. Harris, K. J. Millman, S. J. van der Walt, et al., "Array programming with NumPy," Nature, Vol. 585, pp. 357–362 (Sep. 2020), DOI: 10.1038/s41586-020-2649-2

[32]The pandas development team, Pandas-dev/pandas: Pandas, version v2.0.2, (May 2023), Zenodo, DOI: 10.5281/zenodo.7979740

[33]G. Bradski, “The OpenCV Library,” Dr. Dobb’s Journal of Software Tools, (2000)

[34]F. Chollet et al., Keras, https://keras.io (2015)

[35]TensorFlow Developers, Tensorflow, version v2.13.0, (Jul. 2023), Zenodo, DOI: 10.5281/zenodo.8117732

[36]P. Virtanen, R. Gommers, T. E. Oliphant, et al., “SciPy 1.0: fundamental algorithms for scientific computing in Python,” Nature Methods, Vol. 17, pp. 261–272 (2020), DOI: 10.1038/s41592-019- 0686-2

[37]MLflow Project, mlflow, Series of LF Projects, LLC, <https://mlflow.org/>, (24 Oct. 2023)

[38]T. Akiba, S. Sano, T. Yanase, T. Ohta, and M. Koyama, “Optuna: A next-generation hyperparameter optimization framework,” in Proceedings of the 25th ACM SIGKDD International Conference on Knowledge Discovery and Data Mining (2019)

[39]FLIR Systems, Inc., User´s manual FLIR Ax5 series, Electronic Article (2016)

[40]L. Fahrmeir, C. Heumann, R. Künstler, I. Pigeot, and G. Tutz, Statistik: Der Weg zur Datenanalyse, 8th. Springer Spektrum Berlin Heidelberg (2016), ISBN: 978-3-662-50371-3. DOI: 10.1007/978-3-662-50372-0